ADVANCEMENTS ON A SILICON-ON-INSULATOR THERMOELECTRIC SENSOR FOR BIOMEDICAL APPLICATIONS

by

Alexis Corda

A Thesis

Submitted to the Faculty of Purdue University

In Partial Fulfillment of the Requirements for the degree of

Master of Science in Materials Engineering

School of Materials Engineering

West Lafayette, Indiana

May 2021

THE PURDUE UNIVERSITY GRADUATE SCHOOL
STATEMENT OF COMMITTEE APPROVAL

Dr. Luna Lu, Chair

School of Civil Engineering

Dr. Christopher Emery

Department of Pathology and Laboratory Medicine, IUSOM

Dr. Lia Stanciu

School of Materials Science and Engineering

Approved by:

Dr. David F. Bahr

I dedicate this thesis to my friends and family. Special dedications to Stiven for being there each step of the way and for all the advice and to my parents for encouraging my education and helping me out when I needed it.

ACKNOWLEDGMENTS

I am very thankful for Dr. Luna Lu, my advisor and graduate school mentor. Thank you, Dr. Lu, for your guidance and for molding me into a well-rounded researcher. Through the challenges of the pandemic especially you have continued to support me and this work. Thank you, Dr. Chris Emery, and IUSOM for funding me and this project. Your support and optimism have encouraged much progress. Finally thank you, Dr. Lia Stanciu, for your support and for creating the Biomaterials course which increased my interest in these merging fields.

I would also like to thank Dr. Joon Park and every cleanroom engineer that trained me on equipment and taught me tips and tricks for better fabrication.

Finally, thank you to everyone in Dr. Luna's group. You are all great collaborators and friends.

TABLE OF CONTENTS

LIST OF TABLES

LIST OF FIGURES

ABSTRACT

Heat can be used as a reliable biomarker of cell metabolism. Assessing changes in metabolic activity is useful to study normal bioactivity or factors which may stimulate or inhibit cell proliferation. Methods which measure the heat of cell metabolism over time must be sensitive to the small changes. Thermoelectric sensors, which work by the Seebeck effect, are one method which has shown adequate sensitivity. This type of sensor directly converts heat energy into electrical energy without the use of a power source. Current research into sensors for cell metabolism may list lengthy, complex, and expensive procedures or include materials with rare or toxic elements. This work establishes a design approach of a silicon-based thermoelectric sensor for cell metabolism measurement which incorporates abundant and non-toxic materials and a simple procedure based on standard MEMS fabrication methods. The foundation for the sensor design is discussed. Fabrication was done using optical lithography, reactive ion etching, and electron beam evaporation which are standard and well known in industry. Sensor quality was characterized successfully based on the defined design parameters. Preliminary data has been recorded on the sensor's performance measuring heat production of Escherichia Coli cell metabolism. Finally, recommendations to improve heat insulation, include sensor calibration, and optimize manufacturing parameters are given for future work on this design to advance sensitivity and commercial potential.

1. INTRODUCTION

1.1 Motivation

Thermoelectric sensors have been used to study biochemical processes including enzyme catalyzed reactions and metabolic activities in living cells. By directly measuring heat production as changes in temperature these sensors can identify molecular constituents, understand limiting and promoting effects on cell bioactivity, and determine reaction mechanisms. Thermoelectric sensors for biochemical processes commonly contain a thermopile component consisting of the sensor materials and a microfluidic component for controlling the analyte fluid. The upper limit of each sensor's sensitivity is its inherent total Seebeck coefficient, thus materials with higher values of this property are often selected. Alloys of bismuth and antimony telluride make up most thermoelectric sensor materials due to their high Seebeck coefficients, but they are rare, expensive, and not easily fabricated by standard MEMS processes [1].

Sensitivity is often reduced by heat loss to the environment and limits of the voltage measurement electronics. The tendency of heat dissipation for small temperature changes is opposed by reducing thermal mass beneath the measuring side of the sensor, with the aid of a heat sink beneath the reference side, or through selection of a low thermal conductivity microfluidic component. However, implementing such methods can include complex and costly fabrication or require expensive and bulky volt measurement tools [1], [2].

This work is a foundation and principles study for the design and development of a silicon-on-insulator (SOI) based thermoelectric biosensor which focuses on standard MEMS materials and processes.

1.2 Scope of Thesis

The wide application potential for thermoelectric biosensors has encouraged considerable research into optimal material selection and fabrication methods. To reach industry, the materials should be widely available, cost-effective, and preferably non-toxic. Standardized fabrication methods would allow for a rapid and efficient transition to large scale production. While exploring new fabrication techniques, the design of the thermoelectric biosensor discussed here has been bound by the above-mentioned criteria.

Thermoelectric sensors with these qualities have been developed and reported in literature, however none have been fabricated in the manner discussed in this thesis. This sensor focuses on just three standard MEMS fabrication equipment: reactive ion etching (RIE), optical lithography, and e-beam evaporation. Here the complexities and expenses associated with ion implantation and microfluidic flow regulators are disregarded.

The target application of this sensor is the closed and static measurement of heat production during cell metabolism. Thermoelectric sensors have before been used for this application, thus providing guidelines for sensitivity. Investigating viability by this means allows the avoidance of bioreceptor immobilization such as an enzyme or antibody. Therefore, problems such as bioreceptor density/orientation or enzyme sensitivities to process conditions are bypassed entirely. While the scope of this work is not yet narrowed to rapid measurement of changes in cell metabolism, this direction and its potential implications to the healthcare industry are discussed.

2. LITERATURE REVIEW

2.1 Fundamentals of Thermoelectricity

2.1.1 Seebeck Effect

Thermoelectricity describes the direct conversion between electrical charge movement and a gradient of temperature. When the applied electrical charge movement is responsible for the creation of a temperature gradient, the resulting phenomenon is called the Peltier effect. However, it is the Seebeck phenomenon which will allow for the measurement of heat. It contains the Seebeck coefficient (S) which was discovered by Thomas Johann Seebeck in 1822 and is described by $S = \frac{\Delta V}{\Delta T}$ where the temperature difference (ΔT) is responsible for the voltage difference (ΔV) [3]. Also called thermopower, the Seebeck coefficient is a material property that describes the magnitude of electrical charge carrier movement in response to a difference in temperature. The value can be positive or negative depending on the sign of the free charge carriers (negative for majority electrons and positive for holes).

The Seebeck coefficient is strongly dependent on the material's Fermi level, E_F and is higher when E_F has a larger separation from the conduction or valence band depending on the

charge carrier type. Equations 1 and 2 show the Seebeck coefficient for non-degenerative semiconductors (moderately doped) and for insulators respectively [4], [5].

Equation 1

$$S = \frac{k_B}{e}\left(\frac{E_F - E_c}{k_B T} + A\right)$$

Equation 2

$$S = \frac{k_B}{e}\left(\frac{-E_F}{k_B T} + A\right)$$

In these equations k_B is the Boltzmann constant, e is the electron charge, E_F and E_c are the Fermi and conduction band energy levels, T is the temperature, and A is a constant dependent upon scattering.

From these equations we can assume that insulators have the highest Seebeck coefficients as the magnitude E_F is larger than that of E_F - E_c. However, the Seebeck coefficient of insulators is not commonly reported as they lack sufficient electrical conductivity to provide for a quick and accurate measurement. The low electrical conductivity is attributable to insulators having no free electrons as they are tightly bound to their atoms. On the other hand, for non-degenerative semiconductors a large thermopower depends on a high separation of n-type and p-type charge carriers and on possession of a singular carrier type [5].

The overall thermopower can be increased by joining opposite signed Seebeck coefficient materials at only the positions corresponding to the greatest gradient in temperature (the “hot” and “cold” sides as referenced later). This joining is the basis of the common thermocouple. Combining thermocouples in series creates a thermopile and further multiplies the total Seebeck coefficient by the number of thermocouples in series. Thermopiles are often required when the temperature difference is very small.

2.1.2 Electrical Conductivity

Briefly, the electrical conductivity describes the ease of which charge carriers can move through the material. The higher the electrical conductivity, the higher the efficiency of the thermocouple. Insulators have very low electrical conductivity due to their wide energy band gaps which make promoting charge carriers to the conduction band very energy intensive.

2.1.3 Thermal Conductivity

Thermal conductivity is especially important when the heat source, and thus the change in temperature, are small. A material with a high thermal conductivity will dissipate heat through its bulk and lessen the difference at the junctions. Therefore, materials with low thermal conductivities are often suggested for thermoelectric applications. Often materials with high Seebeck coefficients and high electrical conductivities have low thermal conductivities. Research into the lowering the thermal conductivity of methods of lowering thermal conductivities of these materials is wide and examples of silicon will be discussed below in Thermal Insulation Strategies in Silicon-based Thermoelectric Sensors.

2.2 Thermoelectric Sensors

Thermoelectric sensors are used to recognize heat energy through the display of electrical signal. The heat energy must give rise to a temperature difference across the sensor and a voltage logger should be connected to the hot and cold points. Methods of heat containment at the hot side and excess heat dissipation at the cold side are necessary in the design to maintain the temperature difference. Therefore, materials that often make good thermoelectric sensors are those with high Seebeck coefficients and electrical conductivities, but low thermal conductivities. Current leading thermoelectric materials often contain rare-earth elements or are toxic to health or the environment [6].

The sensitivity of a thermoelectric sensor is dependent upon its total Seebeck coefficient. Theoretically speaking, the higher our thermoelectric sensor's Seebeck coefficient, the smaller the heat release we can measure.

2.3 Silicon-based Thermoelectric Sensors

Silicon is a narrow band gap semiconductor with a large Seebeck coefficient in the range of $|400 - 1000|$ μV/K depending on doping levels [7]. Single crystal silicon is reported to have the highest Seebeck coefficient of any thermoelectric material [8]. In addition, silicon is an abundant material which has good production scalability unlike conventional thermoelectric materials.

Both p-type and n-type silicon have been used to create thermopile sensors. When pairing another material with doped silicon, ohmic contact is important. Ohmic contact follows Ohm's law (V=IR) and moreover has no barrier to electron movement at the interface. It is determined by the joining of the materials' work functions. The work function of any material is defined as the minimum energy required to propel an electron to vacuum as described in $\Phi = E_{vacuum} - E_{Fermi}$. In context, the energy of the vacuum, E_{vacuum}, regards that an electron of the atom is free. In other words, the atom has been ionized. For a metal, the Fermi level, E_{Fermi}, establishes that any energy level below is regarded as a sea of free electrons. Because of this sea, metals are conductive. However, for semiconductors and insulators, the Fermi level establishes a different meaning. In these materials, the Fermi level exists within the band gap and represents the level at which charge carriers have a 50% chance of occupancy. Ideally, the Fermi level of the contact metal will have a lower energy configuration than the highest occupied energy level in the sensor. Typically, a metal's Fermi level is at a higher energy than that of an intrinsic (non-doped) semiconductor.

Silicon has a work function between 4.60 and 4.85 eV incorporating intrinsic and extrinsic values [9]. The larger the work function of the metal, the greater the probability of electrons in silicon to be at an energy higher than the metal and thus the better the ohmic contact. The work function of most metals is around 4-5 eV. **Table 1** below shows elements with work functions greater than 4.85 eV.

Table 1: *Work functions of some elements* [9].

Metal	Work Function (eV)
Beryllium	5.0
Cobalt	5.0
Nickel	5.01
Gold	5.10
Selenium	5.11
Platinum	6.35

The limited selection of available contact metals for silicon is not the only nor the most demanding challenge when incorporating this material into thermoelectric sensors. The thermal conductivity of bulk silicon is 141 W/mK [10]. Thus, the high intrinsic sensitivity of silicon-based thermoelectric sensors may be thwarted by rapid heat dissipation through its bulk. However, there are a few strategies to circumvent such issue.

2.3.1 Thermal Insulation Strategies in Silicon-based Thermoelectric Sensors

Thermal conductivity, like many material properties, is altered when the material enters the nanoscale. Reducing the thickness of silicon directly reduces the thermal conductivity by increasing phonon boundary scattering [11].

Fabricating a thermopile on a SOI wafer is a technique which has been used to create high sensitivity thermoelectric sensors with low silicon thermal conductivity. SOI wafers have a buried oxide sandwiched between a thin layer of silicon and the bulk substrate. With this design the buried oxide's low thermal conductivity acts as a thermal barrier [12]. Asheghi et al graphed room temperature thermal conductivity data for bulk silicon and SOI films between 0.01 to 50 μm [11]. They found no significant difference in thermal conductivity from bulk until films were below 1.5 μm and further explained that films of 0.5 μm or less experienced a reduction over 40% due to phonon boundary scattering [11]. Decreasing from 0.1 μm will continue to reduce the thermal conductivity, but it is at this point when the internal resistance will begin to affect the ability to record a signal [13]. Reducing the thickness is thus crucial for reducing the thermal conductivity yet one can be assured that the nanoscale silicon has the same Seebeck coefficient as the bulk. Salleh et al. explained that a silicon film as thin as 6 nm would have a Seebeck coefficient the same as the silicon wafer, and that doping concentration is the more important influencer on Seebeck coefficient [14].

There also exist methods to control the temperatures at the reference and measuring junctions. The reference junctions should remain at a constant temperature so that changes in ΔT, and thus in ΔV, solely reflect upon the changes of the measuring junction. High thermally conductive heat sinks have been connected to the reference junctions for maintaining their temperature. Bulk silicon and aluminum have been used in thermoelectric biosensors for this purpose [15], [16]. Other publications choose to leave out this design choice either to reduce complexity or perhaps because heat sinks may be less helpful than previously thought. A 2021 paper by Bari, Reis, and Nestorova numerically considered parameters which affect the sensitivity of thermoelectric sensors [17]. Their simulations concluded that the presence of a heat sink reduced the overall temperature difference between the junctions because heat that dissipated from the reaction zone was absorbed by the heat sink [17].

On the other hand, the temperature at the measuring junctions should be influenceable only by the analyte. Thermal insulation of the measuring junctions is thus especially important.

The suspension of the measuring junctions over a membrane is a common strategy which improves the integrity of the temperature difference by removing the thermal mass beneath these junctions [18]. The low thermal conductivity of air (0.0261 W/mK [19]) aids in this environmental separation [16]. The removal of bulk silicon on the backside of the wafer is performed by either wet anisotropic etching or deep reactive ion etching (DRIE).

Material choice to encapsulate or channel the biological fluid also has important implications for the thermoelectric signal. This is the component for microfluidic channels, reaction chambers, and/or membrane insulators. Thermal conductivity is a main consideration when deciding which material to use. The thermal conductivity values for materials which have been used for this purpose in thermoelectric devices are listed in

Table 2.

Table 2: *Thermal conductivities of microfluidic components* [10], [20].

Material	Thermal Conductivity (W/mK)
Glass	1.7
PMMA	0.17 - 0.25
Silicon Nitride	29
PDMS	0.15
PTFE	0.25

A material with a higher thermal conductivity will have faster heat dissipation to the environment and result in a lower temperature difference between the junctions. Although silicon nitride has a much higher thermal conductivity than the rest, this material has been used for its ease-of-application in standard processing. Xensor corporation also explains silicon nitride's stability even with repeated enzyme immobilization or other coatings [21]. While PDMS may have the lowest thermal conductivity, it may be that it can absorb small hydrophobic molecules which would not be beneficial when hydrophobic heat sources such as certain proteins or bacteria are of interest [22]. However, PDMS still remains a generally utilized microfluidic material [23].

2.4 Heat from Cell Metabolism

Heat is a beneficial signal relating to cell metabolism because it is directly related to cell metabolism and does not require enzymes to catalyze a reaction or invasive labeling as do other

methods which estimate metabolic activity such as oxygen consumption, measure an enzyme's activity, or tracks ATP consumption [24].

The use of changes in heat to reference cell metabolism has many practical applications including identifying cells based on their bioactivity as well as understanding effects on it [25]. Metabolic activities including chemical and physical processes lead to heat generation or absorption with heat generation linked inversely to the growth rate [26]–[29]. Therefore, when the growth rate is high, the overall heat production is low [28]. The non-growth-related processes which result in measurable heat include the constant movement of cells, macromolecular turnover, and the preservation of ion gradients across their membranes [29]. The quantity of heat dissipated during these processes will vary depending on the cell's doubling time, the nutrients present, and other environmental conditions [28]. For example, the doubling time of Escherichia Coli is listed at about 17 minutes under optimal conditions while the doubling time of gut bacteria in Mammalia is listed as 2.7 – 2.9 hours (162 – 174 minutes) [28]. E. Coli was reported to produce 739.4 kJ/mol of heat measured by microcalorimetry which can be roughly estimated as $8.03x10^{-3}$ -$1.1x10^{-2}$ kcal/g when estimating E. Coli's molecular weight as between 16 – 22 kDa [30], [31]. Two types of Mammalia gut bacteria are reported to have produced 4.61 kcal/g and 4.78 kcal/g of heat by flow calorimetry [29]. The difference in doubling time may be a reason these bacteria show 2-3 orders of magnitude different heat production.

A sensor which can accurately measure the heat release of a variety of cell types despite known variability of heat production would have the best potential for industry. Considerable studies assess viability with E. coli due to the abundance of literature on these bacteria, its ability to grow in many environments, and the wide range of growth rates that it possesses [15]. For instance, altering the energy source can influence E. Coli's growth rate nearly 10-fold [29]. With this range of growth rates, a sensor can tune the optimal sensitivity towards several specific heat outputs by using only one strain.

Compared with various cells, bacteria have some of the lowest average heat production per cell [32]. which may stand as a standard minimum for sensitivity amongst cell metabolism sensors. A book published by Wright in 1987 contains thermal studies of biological systems that list bacterial heat outputs no greater than 5 pW/cell and although some human blood cells produce less heat (~10^{-3} pW/cell), most other cells including fungal and tissue cells produce heat in the range of 40 – 80 pW/cell [32].

Many papers can be found which use heat production changes in E. Coli as helpful information for the healthcare industry. Measured changes in heat output have been used to estimate the concentrations of Cu^{2+} or La^{3+} which stimulate or become toxic to living organisms [33], [34]. Heat changes of E. Coli have also been used to identify antimicrobial materials by comparing the lag time until the culture reaches the growth stage and the total heat measured for conditions with and without a suspected antimicrobial material [35].

2.5 Thermoelectric Sensors for E. Coli Metabolism

Isothermal microcalorimetry (IMC) is an established tool for measuring energy released in a closed and isothermal system. Although IMC accurately measures the heat of cell metabolism with little heat loss, there are several driving factors which further interest in the research of thermoelectric chip sensing. Most of the driving factors can be related to lowering costs. These include lowering the sample volume and saving time with quicker equilibration [36]. A reduction in the required sample volume would save the cost of an expensive sample or one low in target analyte. A low-grade sepsis sample may have <10 CFU/ml while high-grade bacteremia is considered any concentration >100 CFU/ml [37]. However, current commercial IMC devices are reported to require 100,000 bacteria to measure a signal which would require extensive sampling [38]. The detection limit of IMC for E. Coli specifically has been recorded around 104 CFU [39]. With lower cell detection limits, the speed at which cell metabolism monitoring can provide an analysis is much improved [40]. To achieve high accuracy of results, IMC is typically performed in a closed ampoule. Cell metabolism by aerobic respiration will eventually result in the depletion of oxygen in the ampoule and force the cells to switch their metabolic processes thus affecting the heat production. When this occurs, time to measure the effects on bioactivity and complexity in interpreting the signals are increased. Thermoelectric chip sensing has made strides at improving upon the disadvantages of IMC while remaining sensitive and accurate.

Liu et al used a commercial thermopile sensor by Xensor Corporation to execute E. Coli susceptibility to antibiotics and compare results with gold standard antimicrobial susceptibility testing methods [40]. The sensor is an Al/Si thermopile likely fabricated by MEMS processing; however, the methods are not discussed and the sensors are no longer in production. A data sheet by Xensor reveals a total intrinsic Seebeck coefficient of 50 mV/K and depicts a schematic of the sensor with the measuring junctions over a silicon-nitride membrane to improve thermal insulation

[21]. The authors also sought to improve thermal stability by fabricating a thermostat with heating pads for the reference junctions and by designing a microincubator which put the bacterial solution in direct contact with the thermopile [40]. However, the material of this microincubator nor its thermal conductivity are mentioned. They added 150 μL of an E. Coli suspension with a concentration of about 10^5 CFU/ml, thus the nanocalorimeter measured approximately 15,000 cells [40]. The high sensitivity reported as 1.14 V/W allowed for a shorter analysis of susceptibility (7 h) compared to the gold standard methods (up to 48 h) [40], [41].

Higuera-Guisset et al used the same commercial sensor to measure the cell metabolism of E. Coli, however, they added additional methods of thermal insulation including encapsulating the reaction chamber with PTFE and connecting the reference junctions to an aluminum heat sink [15]. Over 24 hours they measured the heat production of approximately 600 cells in their 0.6 ml PTFE reaction chamber [15]. They list the sensitivity as 1.24 V/W [15]. With the thermopile components from the same source and the sensitivity values determined in a similar manner, it is a reasonable assumption that the 100,000 μV improvement in sensitivity is in large part a result of better thermal insulation strategies.

3. EXPERIMENTAL METHODS

3.1 Sensor Design

3.1.1 Thermopile

Due to aforementioned advantages in Seebeck coefficient, availability, cost, and standardized processing, silicon was the first chosen thermoelectric material. Despite similar properties, p-type silicon (p-Si) was chosen over n-type due to a higher Seebeck coefficient at similar doping concentrations [7]. Nickel (Ni) was chosen as the thermopile's n-type material due to its low cost and higher work function than silicon. Nickel's Seebeck coefficient is near -20 μV/K [42].

To decide the number of thermocouples in the thermopile, the intrinsic sensitivity of the E. Coli metabolic thermoelectric sensor by Higuera-Guisset et al was used as a guideline. Higuera-Guisset et al purchased their silicon-aluminum thermopile from Xensor Integration who lists the device's intrinsic sensitivity as 50 mV/K [21].

If we assume a 500 μV/K Seebeck coefficient for silicon and -20 μV/K for nickel, then around 96 thermocouples would be required to achieve the same sensitivity. During the design, the number of thermocouples settled at 102 and thus has a slightly higher intrinsic Seebeck coefficient.

The dimensions of the thermopile were determined next. The thermopile length (distance between hot and cold junctions) must be large enough to prevent heat from the reaction zone from influencing the temperature at the reference zone, yet it must be small enough for resistance of the legs to not greatly interfere with sensitivity [43]. However, many distances have been used successfully in literature and the optimal length will depend on the other dimensions of the thermopile, the magnitude of heat source, and thermal insulation strategies. To start, 500 μm lengths were chosen. A successful thermoelectric device has been conceived by de Leon et al with legs of length 500 μm when the membrane diameter and thickness were 1 mm and 15 μm respectively [44]. **Figure 1** shows the design of our thermopile.

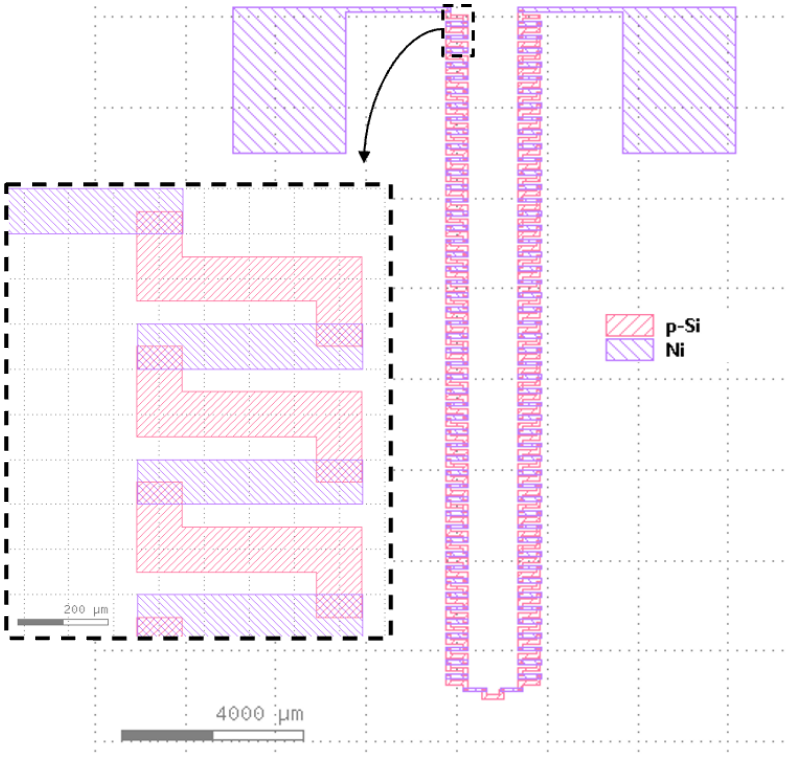

Figure 1: Schematic of thermopile with 102 p-Si/Ni thermocouples.

The p-Si legs are electrically isolated from each other. Each nickel leg overlaps p-Si in an area of 50 µm to ensure contact. Nickel is deposited in two large areas for creating voltmeter contacts to the measuring and reference junctions. The inner distance from the hot junctions on the left to those on the right is 1.3 mm and the total length is 15 mm which creates a large surface area for the fluid heat source.

In this design the biological fluid heat source is meant to be in direct contact with the thermopile, thus maximizing the heat transfer [40]. Alternatively, some thermoelectric sensors may separate the thermopile materials from the fluid heat source for better fluid flow or because their thermopile materials contain elements which are toxic to biological substances.

3.1.2 Thermal Insulation Mechanisms

The decision of silicon as one of the thermoelectric materials thus required the design of thermal insulation mechanisms.

The thermopile was designed for creation upon a SOI wafer. The thickness of the buried oxide was not of particular importance as the bulk value of SiO_2 thermal conductivity is low enough to cause sufficient boundary scattering [12] and approaching the nanoscale would only reduce the thermal conductivity [45]. The target thickness for p-Si is less than 1 μm to significantly reduce the thermal conductivity.

Creation of a membrane for the measuring junctions by etching the backside to the buried oxide was included in the initial design to reduce the thermal mass beneath the measuring junctions and thermally isolate them from the environment. However, testing of heat production from cell metabolism was performed with sensors lacking this feature due to time restrictions. In their data sheet, Xensor mentions the purpose of the membrane was for improving the thermal resistance of moving liquids [21]. While likely to improve the temperature difference, creating the membrane structure may not be necessary for our sensor in static conditions.

PDMS is chosen as the material to form into the reaction chamber for holding the analyte fluid due to its low thermal conductivity, ease-of-use, and availability in our lab. Because we plan to test cell metabolism with a relatively large concentration of bacteria, we are not concerned with possible absorption effects at this time. The mold for creation of the PDMS reaction chamber is shown in **Figure 2**.

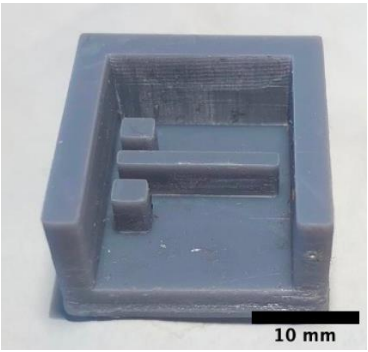

Figure 2: Resin 3D printed mold for the PDMS reaction chamber.

This mold has three walls and tapered edges for easy removal of PDMS after curing. The reaction chamber is the middle feature and is 15 x 1.5 x 5 mm. Two squares of 3 x 2 mm are included in the design in the same positions as the contact pads for easy connection to the voltmeter.

3.2 Sensor Fabrication

SOI wafers were purchased from Siegert Wafer with a 4.6 ± 0.4 µm boron doped device layer (1-5 Ωcm) and a BOX thickness of 2.1 µm ± 0.5%. Pieces were cut from the wafers and cleaned by sonication for 5 minutes sequentially in acetone, methanol, and isopropyl alcohol. An overview of fabrication is visualized in the flow chart in **Figure 3**. The pathways consist of fabrication methods for the thermopile and microfluidic components which converge upon their adhesion to each other. Specific processes of thermopile fabrication are only briefly mentioned in the flow chart with white arrows branched off main concepts.

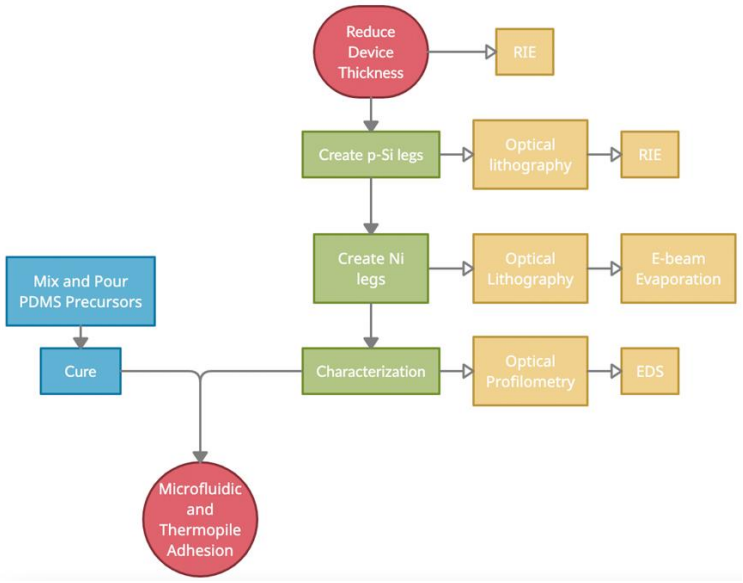

Figure 3: Fabrication flow chart where red indicates start and stop, blue indicates microfluidic processes, green indicates thermopile processes, and yellow details thermopile processes.

Prior to patterning the p-Si legs, the pieces required etching to reduce the device layer thickness. One of the pieces was used to determine an appropriate etching time. This piece was dried for 5 minutes at 130°C before spin coating a layer of AZ® 9260 at 3800 rpm for 45 seconds. The piece was soft baked then a pattern containing several squares of 1 mm, 100 µm, and 10 µm was exposed in the Heidelberg MLA150 at a dose of 900 mJ/cm^2 and developed in AZ 400K for 10 seconds. The piece was then etched in the March Jupiter II reactive ion etcher (RIE) for 3.5 minutes with SF_6 gas at a flow rate of 10 sccm and a forward power of 100 W. This gas was chosen as it is non-toxic and has a silicon to oxide selectivity between 10:1 and 100:1 [46] thus the buried

oxide may act as an etching stop layer until the silicon pattern is etched to completion. After etching, the piece was cleaned and the process was repeated for every 30 second etching times from 4 to 6 minutes.

After choosing the appropriate non-masked etch time, pieces were prepared for creation of the p-Si legs. The p-Si pattern shown in **Figure 1** was developed and etched with the same parameters until the buried oxide was exposed around the legs as confirmed by a colored reflection. The Bruker GT-K optical profilometer was used to approximate the feature heights.

The same process was used to pattern the Ni legs. After developing, the sensors were dipped in buffered oxide etch (BOE) for 10 seconds to remove the native oxide then rinsed and loaded into the PVD E-beam Evaporator System and Ni was deposited at a rate of 2 Å/s. Metal lift-off was performed by immersion in acetone and sonication for 1 minute. A silicone elastomer kit was purchased by Sylgard® and mixed in 10:1 ratio of PDMS to curing agent. A desiccator was used to remove all bubbles before pouring the mixture into the mold shown in **Figure 2Error! Reference source not found.**. PDMS was cured on a hot plate at 65°C for 2 hours.

Adhesion of the PDMS microfluidic to the thermopile was trialed first with oxygen plasma on the surfaces which will make contact. The March Jupiter II was used with an O_2 flow rate of 20 sccm and 60 W forward power for 30 seconds. Adhesion should be promoted by the removal of contaminants and the conversion of methyl side chains in PDMS to silanol groups [47]. However, adhesion was not successful, potentially due to microroughness on the surface of the buried oxide occurring upon oxide growth. Oxidizing the surface with a corona wand to promote adhesion was also unsuccessful. Thus, in the interest of time, tape was placed by eye over the measuring junctions and the voltmeter contacts and a thin layer of 100% silicone adhesive by GE was smeared on the thermopile. The microfluidic was gently placed by eye and the sensor was cured in the oven at 70°C for 1 hour.

3.3 Boiling Water Heat Sensing

To gauge the linearity and sensitivity of the voltage response to a change in temperature, boiling water was added via needle injection to the reaction chamber while change in voltage was continuously measured. Three injections of 35 µl were added at times 0, 30, and 50 minutes. Therefore, the reaction chamber would not overflow. The change in voltage for this experiment was compared with that from measuring a blank for one hour.

3.4 E. Coli Metabolism Heat Sensing

Preliminary tests on the sensitivity of the thermopile to the heat produced from cell metabolism was done by continuous voltage collection by the Picolog ADC-20 voltage logger. E. Coli 25922 was grown overnight at 37°C and suspended in a saline solution at a concentration of roughly 10^8 CFU/ml as inferred from a 0.5 MacFarland optical measurement. The solution was then mixed 3:1 with tryptic soy broth. Volumes of 100 µl of the mixed solution were injected into the reaction chambers of two identical sensors and voltage measurements were taken every 30 seconds over 3 hours.

4. RESULTS AND DISCUSSION

4.1 Reactive Ion Etching

Optical profilometry and energy dispersive spectroscopy (EDS) were used to determine the appropriate etching time before patterning with the piece that was patterned with 1 mm, 100 μm, and 10 μm squares. Etching depth of the 100 μm squares etched every 30 seconds from 3 min 30 seconds to 6 minutes was estimated from an image of optical profilometry as shown in **Figure 4**.

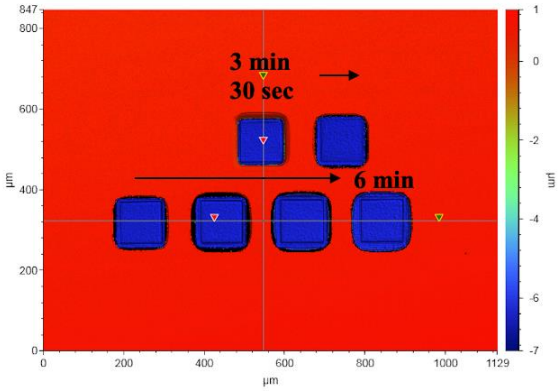

Figure 4: Image from the Bruker GT-K optical profilometer of 100 um squares etched for different times.

Regardless of etching time, each square has relatively the same etch depth of ~7 μm. The features appear colored as to indicate the buried oxide layer, however, the device layer of the wafer should be only 4.6 μm. An etching depth of 7 um would indicate etching had been deeper than the 4.6 μm device layer and the 2.1 μm buried oxide. EDS was used to determine the elements present in the etched squares. Weight percentage data from EDS is shown in **Table 3**.

Table 3: *EDS data from 100 μm squares etched by SF_6 plasma for different times.*

Etch Time	Weight %		Error %	
	O	Si	O	Si
3 min 30 sec	42.23	57.77	5.19	1.76
4 min	42.67	57.33	5.17	1.77
4 min 30 sec	42.67	57.33	5.17	1.77
5 min	42.61	57.39	5.17	1.77
5 min 30 sec	42.57	57.43	5.17	1.77
6 min	42.47	57.53	5.18	1.77
Unetched	-	100	-	1.57

Evidence from **Table 3** reveals that the buried oxide was exposed, and not etched through. However, all the etching times reveal that the entire 4.6 μm of the device layer were etched completely after only 3.5 minutes. This disagrees with visual clues from etching 5 minutes with the same parameters on a non-masked piece. The non-masked piece was not entirely color reflective, indicating the buried oxide had not been reached. The reason for the disagreement is the wide difference in exposed silicon. The bare silicon piece has 25 mm^2 of exposed silicon. Less than 1% of that area is exposed for each etching time. The etch rate for silicon is thus increased upon this decrease in the exposed silicon. Thus, the appropriate etching time prior to p-Si patterning was determined by varying the etching times of a fully exposed (non-masked) 25 mm^2 piece followed by etching of the p-Si leg pattern. The optical profilometry images for various times of non-masked etching followed by p-Si pattern etching is shown in **Figure 5**.

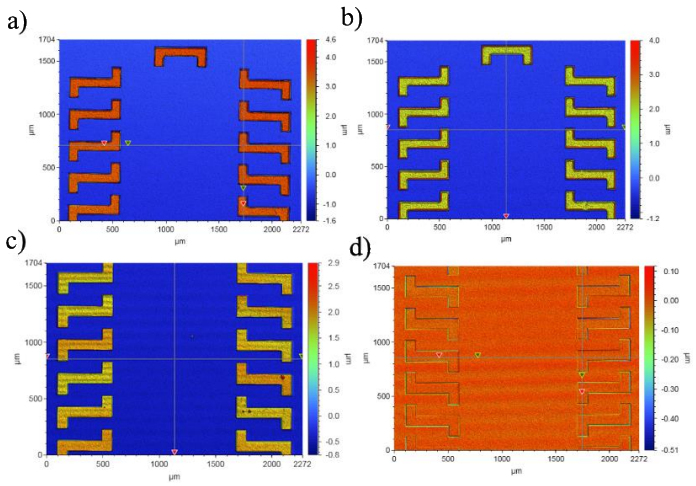

Figure 5: Optical profilometry of pieces following varying non-masked etching times and etching of the p-Si leg pattern to the buried oxide. Bare etching times vary as a) 3 minutes, b) 4 minutes, c) 5 minutes, d) 6 minutes.

Figure 5 shows that for increasing non-masked etching times, the p-Si legs decrease in thickness difference from the buried oxide layer. There is a decrease from about 4.2 μm for 3 minutes of bare etching to about 5.8 nm for 6 minutes of non-masked etching. However, differences in the wafer shown in **Figure 5.d** are so small that the error of uniformity of 400 nm in the original wafer has likely led to areas of no device layer silicon although this was not confirmed by EDS. This data suggests that about 5 minutes is the appropriate bare etching time of a single piece. When production increases to create more sensors, the area exposed increases and the etch rate decreases. Therefore, the ultimate non-masked etch time was determined as 5 minutes and 30 seconds for the batch processing of 3 wafers.

4.2 Electron Beam Evaporation

The first two trials of Ni deposition did not result in proper Ni adhesion to the buried oxide layer despite making changes to the photoresist. The challenges associated with these depositions can be understood by the images in **Figure 6**.

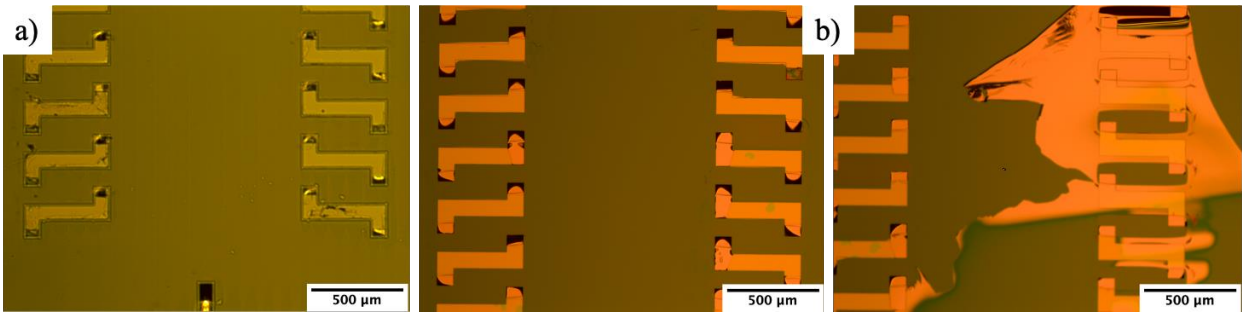

Figure 6: Optical images after Ni deposition by Magnetron Sputtering for a) trial one and b) trial two.

Each image in **Figure 6** shows a failure of Ni to adhere to the buried oxide layer while adhesion is visible on the p-Si legs. Issues with metal lift-off are also shown in **Figure 5.b**. Areas such as this have been found in each sensor of trials one and two suggesting a need for a change in procedure.

To improve Ni deposition on SiO_2, a thin layer of titanium (Ti) was deposited on the buried oxide prior to Ni deposition. However, because Ti has a lower work function than p-Si, charge carriers would not easily flow into it. Therefore, it was important to design a new mask that avoided depositing Ti in between the layers of p-Si and Ni at the junction. The design of the new mask is shown in **Figure 7**.

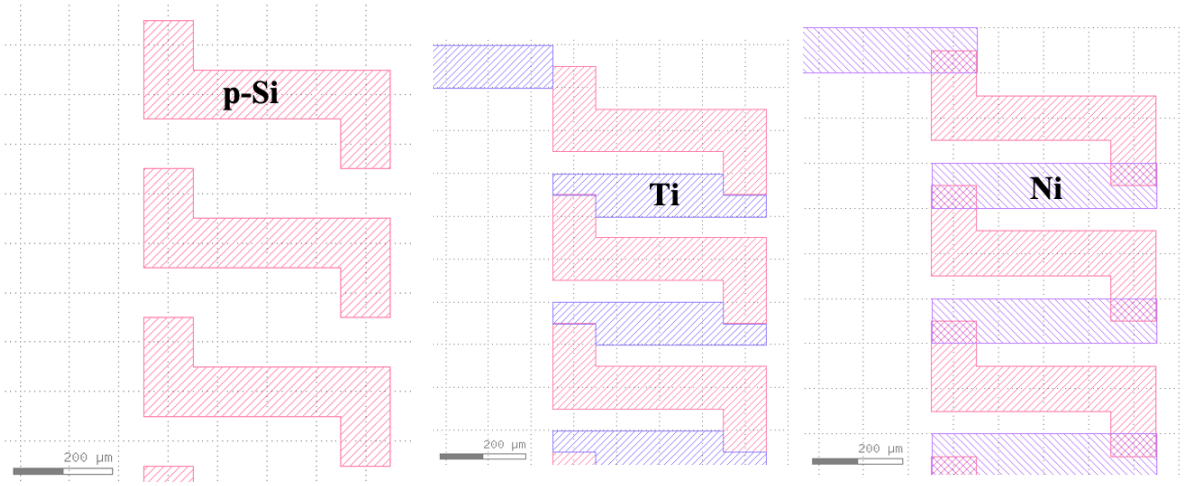

Figure 7: Schematic of the Ti mask showing no deposition on top of the p-Si legs.

A layer of 100 nm Ti was deposited at a rate of 2 Å/s and adhesion to the buried oxide was confirmed before Ni deposition. Optical images after Ti deposition are shown in **Figure 8**.

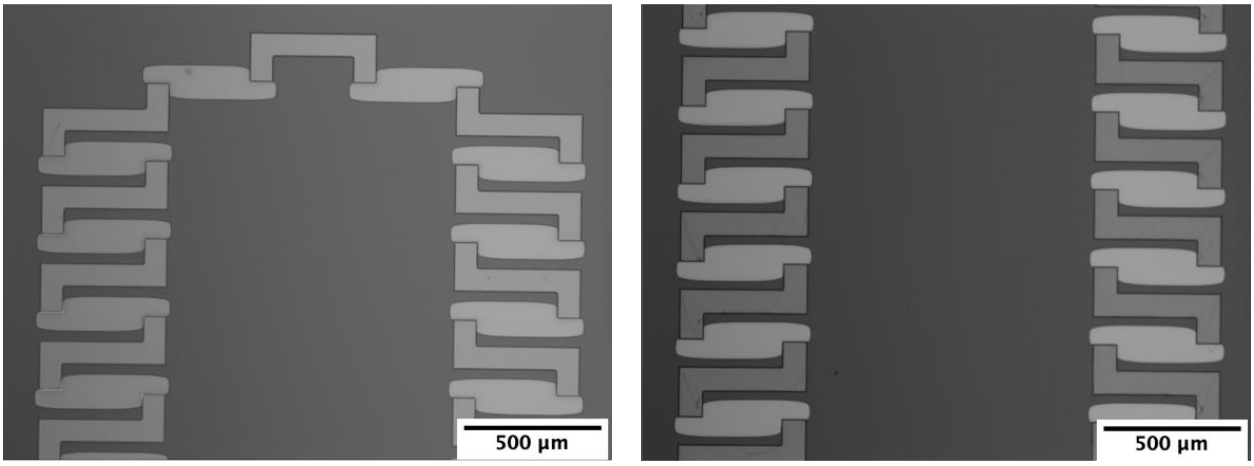

Figure 8: Optical images showing Ti deposition.

Avoidance of Ti on the regions of the Ni/p-Si junctions was confirmed by images in **Figure 8**. The slightly bulged deposition seen in these images is likely a result of over-developing. Issues with metal lift-off were not as apparent in the sensors after Ti deposition. It was determined that the thickness ratio of deposited metal and photoresist was not small enough for successful lift-off of 1 µm of Ni. Thus, the spin coating and lithography procedures moving forward were adjusted to a thicker photoresist deposition.

Following confirmation of Ti adhesion, 100 nm of Ni was deposited in the same pattern and confirmed by EDS as shown in **Figure 9**.

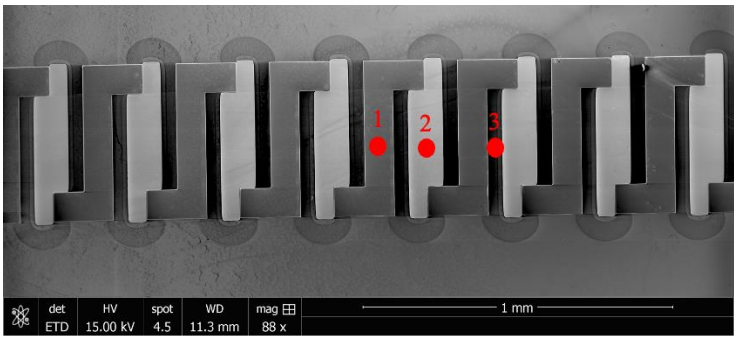

Element	Spot 1	Spot 2	Spot 3
Silicon	**100%** (1.58%)	**21.34%** (3.56%)	**56.88%** (1.79%)
Oxygen	-	-	**43.12%** (5.16%)
Titanium	-	**38.09%** (2.23%)	-
Nickel	-	**40.57%** (3.29%)	-

Figure 9: SEM image and EDS results after 100 nm of Ti and 100 nm Ni deposition in the Ti mask pattern. The information on the right shows element weight percentages with errors included in parentheses.

Spot 1 shows no oxygen content meaning the 5 minute non-masked etch did not reach the buried oxide. Spot 2 shows similar amounts of Ni and Ti as well as a slightly less percentage of silicon. The depth of EDS analysis is about 1-3 μm [48]. Thus, the findings for spot 2 are in line with what should be based on the design of the thermopile. Elemental results for spot 3 are consistent with SiO_2 spots in **Table 3** thus confirming electrical isolation of the p-Si legs.

The third trial of Ni deposition was completed after confirmation of adhesion to Ti. Optical images post lift off are shown in **Figure 10**.

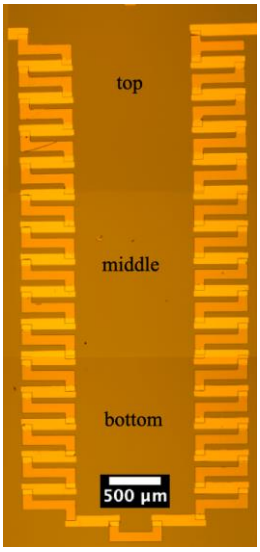

Figure 10: Collaged optical images of the bottom, middle, and top of a sensor following Ni deposition in the Ni leg pattern structured by way of showing the completed thermopile.

Once adjusting the thickness of the photoresist mask to be greater than ¼ of the nickel thickness, metal lift-off had a higher success rate. A sensor was confirmed ready for heat sensing once all junctions were confirmed via optical microscopy.

4.3 Heat Sensing

The data logger used in these experiments is portable and user friendly thereby increasing the potential for easy translation into the healthcare industry. The completed sensor in ambient conditions with contacts is shown in **Figure 11** while the set-up for voltage sensing of cell metabolism at 37°C is shown in **Figure 13**.

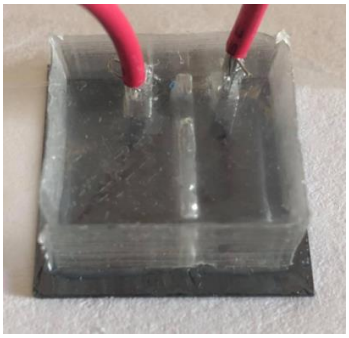

Figure 11: Image of the sensor with insulated wire connections.

Data of voltage background against a sensor with boiling water added to the reaction chamber at times 0, 30, and 50 minutes are shown in **Figure 12**.

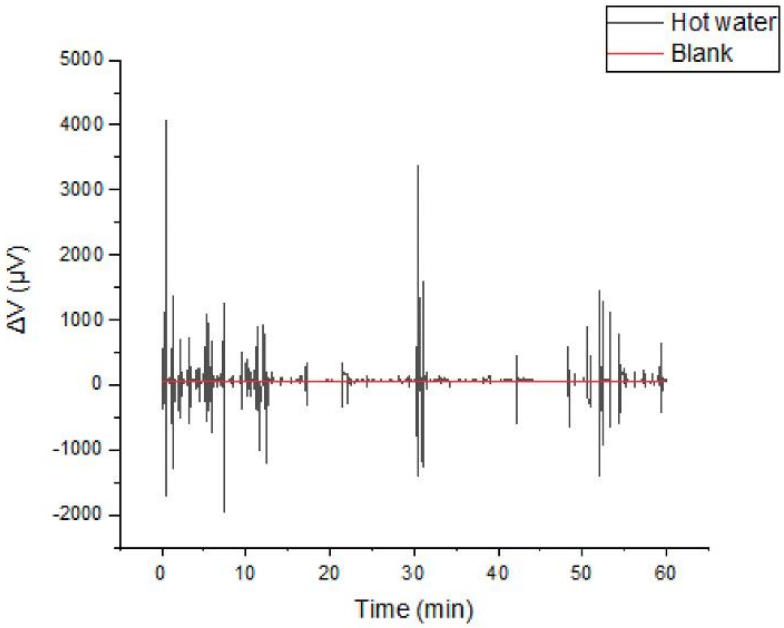

Figure 12: Data from room temperature voltage measurements of (black) boiling water added to the sensor's reaction chamber at times 0, 30, and 50 minutes compared with (red) blank sample over 60 minutes.

The red curve in **Figure 12** which shows data for the blank sample has an average voltage difference of 65.22 μV. Immediately after the addition of boiling water at times 0 and 30 minutes there was a large difference in voltage measured with the largest difference, about 4 mV, after the addition at time 0 minutes. The smaller voltage differences at times 30 and 50 minutes may be due

to the boiling water mixing with room temperature water remaining in the reaction chamber. Because the voltage differences after each addition are not similar and the noise in the measurement creates a curve which does not follow a distinct trend, there is little information we can conclude about the temperature difference due to boiling water. What we can conclude is that the sensor measured differences in voltage in the mV range. There is also little to no drift of the baseline measurement which may be important for recognizing small differences once greater control over the signal to noise ratio is achieved.

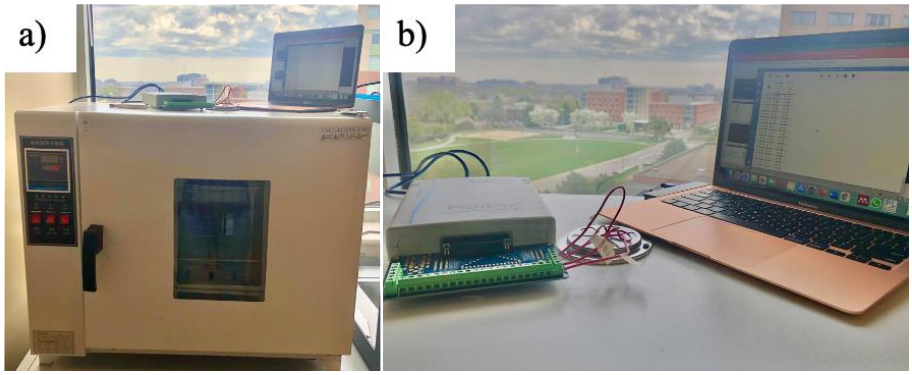

Figure 13: Voltage measurement set-up for sensors in an oven set to 37°C where a) shows the entire set-up, and b) shows a zoomed image on the voltage logger and computer.

The entire sensor is not shown in **Figure 13** because it remains in the oven for cell metabolism sensing.

For the first trial of cell metabolism heat sensing, the sensors were placed in a 37°C oven and brought to a uniform temperature for 10 minutes. Then 100 µl of a mixture of 75% 0.5 MacFarland and 25% tryptic soy broth was added at time 0 minutes. Voltage measurements were taken every 30 seconds over 3 hours on two sensors with the same conditions and data is shown in **Figure 14**.

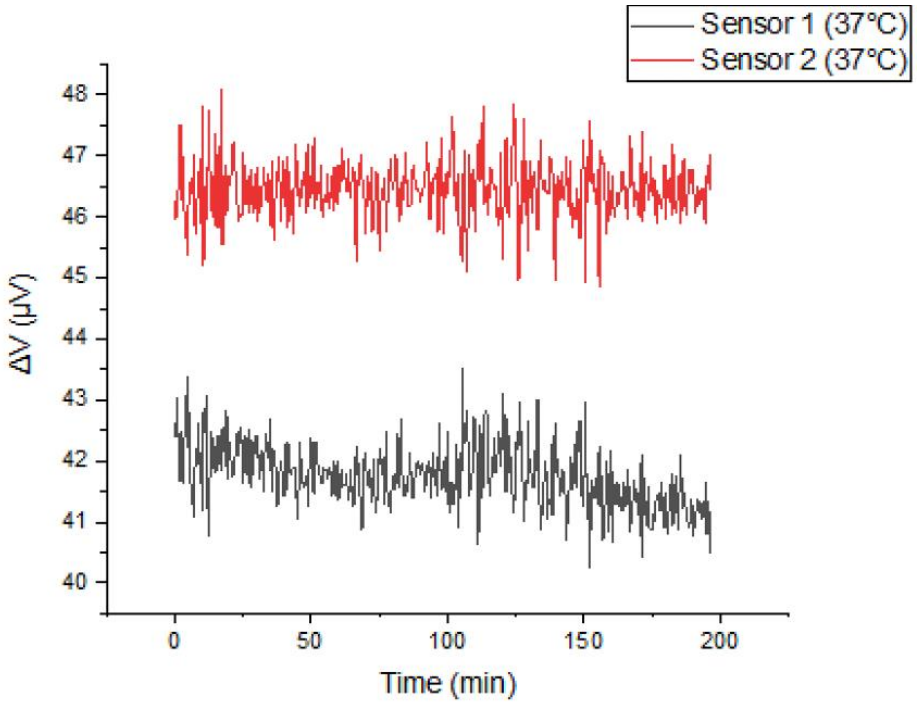

Figure 14: Voltage difference measurements of two identical sensors with 100 µl of a E. Coli 25922 solution over 3 hours at 37°C.

It can be noted that the lag phase before exponential heat production in bacterial cells is known to decrease with a higher concentration of cells [35]. Higuera-Guisset et al. experienced a lag phase of about 7-8 hours when measuring 600 cells of E. Coli [15], thus we would expect a much shorter lag phase when testing with millions of cells. We see no such exponential growth of the voltage curve due to exponential heat flow. Perhaps the oven increases the sinking of heat to the environment, or perhaps the bacterial solution did not remain solely over the measuring junctions due to the sensor not resting flat in the oven. Encouragingly, the voltage response has a clear baseline for each sensor.

5. CONCLUSIONS AND RECOMMENDATIONS

Significant advancements were made on this new SOI thermoelectric biosensor, but this work is only the first step at optimization. This work designed and successfully fabricated the biosensor using three common MEMS equipment: optical lithography, reactive ion etching, and e-beam evaporation. All processes are highly competitive in industry and already may accommodate batch processing. Other major advantages include cost efficient materials and methods and high intrinsic sensitivity. We have concluded that sensitivity and thermal insulation require improvements to recognize heat produced from cell metabolism. The environmental condition of 37°C is optimal for many strains of bacteria and may shorten the time to recognize effects on cell metabolism. This would have many benefits recognizing susceptibility profiles and antimicrobial agents. Recommendations are categorized as either design changes based off fabrication complications or those towards improvement of sensitivity.

5.1 Fabrication Complications

Many procedural optimizations were made during experimental iterations; however, a few changes were not included due to time, and are recommended before future fabrication.

The thickness and uniformity of the SOI device layer is the most important logistical change which should be made to improve the ease of fabrication. By choosing a device layer which is already in the nanoscale and has a smaller variation in thickness will remove completely the step of non-masked etching prior to p-Si leg creation. A nanoscale thickness will also reduce the p-Si pattern etching time which would increase time efficiency for industrial manufacturing. The SOI used in this work was purchased when a greater priority was placed on a backside oxide to eliminate the tools required for growing an oxide necessary for DRIE as explained below in Thermal Insulation Strategies. While the need for DRIE to create a membrane under the measuring junctions has not been certified as unnecessary to the static condition of measuring cell metabolism, a greater priority should now be placed upon a nanoscale device thickness.

The percentage of usable PDMS reaction chambers made from the mold design shown in **Figure 2** was 30% due to difficulties removing PDMS between thin walls. Small alterations such

as widening the distance from the reaction chamber and contacts to the outer walls will likely have a large improvement on the mold's efficiency.

The microfluidic component also requires considerable upgrades to improve the sensing ability. Because this component was not permanently adhered to the sensor, some trials experienced leaking of the analyte fluid. Oxygen plasma has been known to adhere silicon substrates with PDMS upon exposure, but due to a lack of time this process could not be optimized. In addition, a method to accurately place the PDMS reaction chamber should be explored in future works.

5.2 Thermal Insulation Strategies

There may be many reasons which may have led to the inability to measure accurately a signal from cell metabolism due primarily to inadequate thermal insulation strategies.

Additional thermal insulation strategies in the design may be made to contain the heat source near the measuring junctions.

Creating a membrane beneath the measuring junctions is a common strategy by silicon-based thermoelectric sensors and is the first recommendation to the original design for its employment of the low thermal conductivity of air to reduce heat dissipation to the environment. DRIE may be used to create this membrane beneath. The design may look like **Figure 15** below.

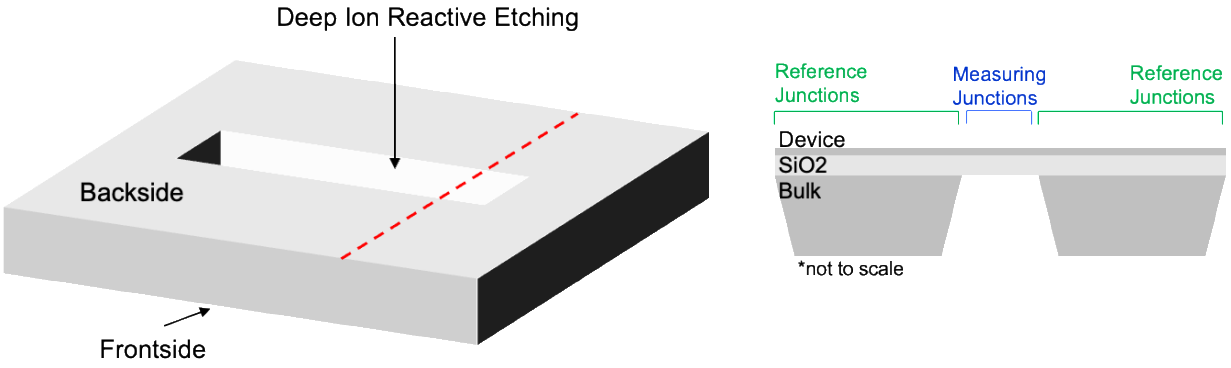

Figure 15: Schematic of the backside view and side view that could be included in the design to improve thermal insulation at the measuring junctions. The red line indicates the point at which the cross section on the right is taken.

It is important to create a trench with walls on all four sides for improved mechanical stability.

The thermopile design may also require optimization in terms of the number of thermocouples and the dimensions. To reach a lower detection limit the number of thermocouples may need to be reduced to reduce the electronic noise [25]. And while 500 μm has been successfully employed as a thermopile length, it may require optimization in the design for a particular application like cell metabolism measurement or for a wider variety of applications.
The publications mentioned in this thesis which have used thermoelectric sensors to measure E. Coli heat release used either a heat sink or heating pads to maintain equilibrium temperature with the environment at the reference junctions [15], [40]. In this design, no external mechanism was created for this purpose which may have affected the temperature difference if the reference junction. Heat from the reaction chamber could have lingered near the reference junction, reducing the sensitivity. As heat sinks have been considered as non-beneficial by simulations of Ishraq Bari, Reis, and Nestorova [[17], this addition may not be first recommended, but considered if the thermal insulation strategies previously mentioned have not allowed for a successful measurement.

5.3 Improving Commercial Potential

A future design update to the device layer should include a more robust means of calibrating the sensor. Other methods have deposited patterns of thermally resistive metals such as nickel which provide uniform and close contact to the measuring junctions [16]. A known amount of power can be supplied to this metal trace which can be used to determine the sensitivity of the thermopile in V/W thus providing a means to characterize the heat production in cell metabolism.

A sensor which may be used repeatedly would greatly improve the cost efficiency and commercial potential. Currently there is not a method designed for rinsing after use which restricts each sensor to one use. The microfluidic component should include a flow inlet and outlet for washing between measurements. This addition will increase complexity slightly, but not to the extent of active flow sensors which must optimize the analyte flow rates for accurate testing.

In this work, heat production from cell metabolism was measured over 3 hours. Ultimately, understanding the metabolic activity and growth stage of cells rapidly with a shorter lag phase is the main future application driving this research. Properly diagnosing and identifying

susceptibility of bacterial strains quicker than modern methods (24 - 48 h) [41] would allow healthcare workers to accurately prescribe antibiotics and help to minimize bacterial resistance.

REFERENCES

[1] D. Assumpcao, S. Kumar, V. Narasimhan, J. Lee, and H. Choo, "High-performance flexible metal-on-silicon thermocouple," *Scientific Reports*, vol. 8, no. 1, pp. 1–10, 2018, doi: 10.1038/s41598-018-32169-9.

[2] V. L. Kopparthy, S. M. Tangutooru, G. G. Nestorova, and E. J. Guilbeau, "Thermoelectric microfluidic sensor for bio-chemical applications," *Sensors and Actuators, B: Chemical*, vol. 166–167, pp. 608–615, 2012, doi: 10.1016/j.snb.2012.03.021.

[3] T. M. Tritt, "Thermoelectric phenomena, materials, and applications," *Annual Review of Materials Research*, vol. 41, pp. 433–448, 2011, doi: 10.1146/annurev-matsci-062910-100453.

[4] H. Fritzsche, "A general expression for the thermoelectric power," *Solid State Communications*, vol. 9, no. 21, pp. 1813–1815, 1971, doi: 10.1016/0038-1098(71)90096-2.

[5] "Thermoelectric Properties of Materials," *Northwestern Materials Science and Engineering*. http://thermoelectrics.matsci.northwestern.edu/thermoelectrics/index.html.

[6] J. H. Yang, Q. Yuan, H. Deng, S. H. Wei, and B. I. Yakobson, "Earth-abundant and non-toxic SiX (X = S, Se) monolayers as highly efficient thermoelectric materials," *Journal of Physical Chemistry C*, vol. 121, no. 1, pp. 123–128, 2017, doi: 10.1021/acs.jpcc.6b10163.

[7] M. Wagner, "Simulation of Thermoelectric Devices," 2007.

[8] W. H. Lee, Y. T. Lee, H. Takao, K. Sawada, and M. Ishida, "Fabrication of thermoelectric sensor using silicon-on-insulator structure," *Japanese Journal of Applied Physics, Part 1: Regular Papers and Short Notes and Review Papers*, vol. 46, no. 11, pp. 7232–7236, 2007, doi: 10.1143/JJAP.46.7232.

[9] D. R. Lide and G. Baysinger, "Physical Constants of Organic Compounds," *CRC Handbook of Chemistry and Physics*, pp. 3-1-3–576, 2019, doi: 10.1201/9781315380476-3.

[10] W. D. Callister and D. G. Rethwisch, "Properties of Selected Engineering Materials," in *Materials Science and Engineering*, 10th ed., Wiley.

[11] M. Asheghi, M. N. Touzelbaev, K. E. Goodson, Y. K. Leung, and S. S. Wong, "Temperature-dependent thermal conductivity of single-crystal silicon layers in soi substrates," *Journal of Heat Transfer*, vol. 120, no. 1, pp. 30–36, 1998, doi: 10.1115/1.2830059.

[12] Y. S. Ju and K. E. Goodson, "Phonon scattering in silicon films with thickness of order 100 nm," *Applied Physics Letters*, vol. 74, no. 20, pp. 3005–3007, 1999, doi: 10.1063/1.123994.

[13] A. P. Perez-Marín *et al.*, "Micropower thermoelectric generator from thin Si membranes," *Nano Energy*, vol. 4. pp. 73–80, 2014, doi: 10.1016/j.nanoen.2013.12.007.

[14] F. Salleh, K. Asai, Akihiro Ishida, and H. Ikeda, "Seebeck coefficient of ultrathin silicon-on-insulator layers," *Applied Physics Express*, vol. 2, no. 7, 2009, doi: 10.1143/APEX.2.071203.

[15] J. Higuera-Guisset, J. Rodríguez-Viejo, M. Chacón, F. J. Muñoz, N. Vigués, and J. Mas, "Calorimetry of microbial growth using a thermopile based microreactor," *Thermochimica Acta*, vol. 427, no. 1–2. pp. 187–191, 2005, doi: 10.1016/j.tca.2004.09.010.

[16] E. A. Johannessen, J. M. R. Weaver, L. Bourova, P. Svoboda, P. H. Cobbold, and J. M. Cooper, "Micromachined nanocalorimetric sensor for ultra-low-volume cell-based assays," *Analytical Chemistry*, vol. 74, no. 9, pp. 2190–2197, 2002, doi: 10.1021/ac011028b.

[17] S. M. Ishraq Bari, L. G. Reis, and G. G. Nestorova, "Numerical Optimization of Key Design Parameters of a Thermoelectric Microfluidic Sensor for Ultrasensitive Detection of Biochemical Analytes," *Journal of Thermal Science and Engineering Applications*, vol. 13, no. 2, 2021, doi: 10.1115/1.4047826.

[18] D. Xu, Y. Wang, B. Xiong, and T. Li, "MEMS-based thermoelectric infrared sensors: A review," *Frontiers of Mechanical Engineering*, vol. 12, no. 4, pp. 557–566, 2017, doi: 10.1007/s11465-017-0441-2.

[19] Engineering ToolBox, "Air - Thermal Conductivity," 2009. https://www.engineeringtoolbox.com/air-properties-viscosity-conductivity-heat-capacity-d_1509.html.

[20] S. Contents and P. Class, "Polymer Data Polymer Data," no. June, 1999.

[21] X. Integration, "Liquid Nanocalorimeter Liquid Nanocalorimeter About this Application Note Short description," vol. 31, no. May 1988, pp. 1–9, 2016.

[22] M. W. Toepke and D. J. Beebe, “PDMS absorption of small molecules and consequences in microfluidic applications,” *Lab on a Chip*, vol. 6, no. 12, pp. 1484–1486, 2006, doi: 10.1039/b612140c.

[23] R. D. A. A. Rajapaksha, N. A. N. Azman, M. N. A. Uda, U. Hashim, S. C. B. Gopinath, and C. A. N. Fernando, “Multichannel PDMS microfluidic based nano-biolab-on-a-chip for medical diagnostics,” *AIP Conference Proceedings*, vol. 2045, no. December, 2018, doi: 10.1063/1.5080833.

[24] “Sugars , lipids , the enzymes of glycolysis , the citric acid cycle , and more.”

[25] S. Wang, X. Sha, S. Yu, and Y. Zhao, “Nanocalorimeters for biomolecular analysis and cell metabolism monitoring,” *Biomicrofluidics*, vol. 14, no. 1, 2020, doi: 10.1063/1.5134870.

[26] A. G. Marr, E. H. Nilson, and D. J. Clark, “THE MAINTENANCE REQUIREMENT OF ESCHERICHIA COLI,” pp. 536–548, 1962.

[27] S. J. Pirt, “The Maintenance Energy of Bacteria in Growing Cultures,” *Proceedings of the Royal Society of London*, vol. 163, no. 991, pp. 224–231, 2016, [Online]. Available: http://www.jstor.org/stable.

[28] E. Rosenberg and I. Ziller-Rosenberg, “Do microbiotas warm their hosts?,” *Gut Microbes*, vol. 7, no. 4, pp. 283–285, 2016.

[29] J. B. Russell, “The energy spilling reactions of bacteria and other organisms,” *Journal of Molecular Microbiology and Biotechnology*, vol. 13, no. 1–3, pp. 1–11, 2007, doi: 10.1159/000103591.

[30] Z. Dermoun and J. P. Belaich, “Microcalorimetric study of Escherichia coli aerobic growth: theoretical aspects of growth on succinic acid,” *Journal of Bacteriology*, vol. 143, no. 2, pp. 742–746, 1980, doi: 10.1128/jb.143.2.742-746.1980.

[31] K. Todar, “The Growth of Bacterial Populations,” in *Todar’s Online Textbook of Bacteriology*, p. 3.

[32] “Thermal and Energetic Studies of Cellular Biological Systems,” *Thermal and Energetic Studies of Cellular Biological Systems*. 1987, doi: 10.1016/c2013-0-06478-x.

[33] Z. Ruming, L. Yi, X. Zhixiong, S. Ping, and Q. Songsheng, “A microcalorimetric method for studying the biological effects of La3+ on Escherichia coli,” *Journal of Biochemical and Biophysical Methods*, vol. 46, pp. 1–9, 2000.

[34] J. Yao *et al.*, "Study of the thermokinetic properties of copper(II) on Escherichia coli growth," *Biological Trace Element Research*, vol. 92, no. 1, pp. 61–69, 2003, doi: 10.1385/BTER:92:1:61.

[35] N. Haman, K. Morozova, G. Tonon, M. Scampicchio, and G. Ferrentino, "Antimicrobial effect of picea abies extracts on e. coli growth," *Molecules*, vol. 24, no. 22, 2019, doi: 10.3390/molecules24224053.

[36] O. Braissant, D. Wirz, B. Göpfert, and A. U. Daniels, "Biomedical use of isothermal microcalorimeters," *Sensors (Switzerland)*, vol. 10, no. 10, pp. 9369–9383, 2010, doi: 10.3390/s101009369.

[37] J. R. Waldeisen, T. Wang, D. Mitra, and L. P. Lee, "A real-time PCR antibiogram for drug-resistant sepsis," *PLoS ONE*, vol. 6, no. 12, 2011, doi: 10.1371/journal.pone.0028528.

[38] O. Braissant, D. Wirz, B. Göpfert, and A. U. Daniels, "Use of isothermal microcalorimetry to monitor microbial activities," *FEMS Microbiology Letters*, vol. 303, no. 1, pp. 1–8, 2010, doi: 10.1111/j.1574-6968.2009.01819.x.

[39] U. von Ah, D. Wirz, and A. Daniels, "Isothermal micro calorimetry a new method for MIC determinations: Results for 12 antibiotics and reference strains of E. coli and S. aureus," *BMC Microbiology*, vol. 9, no. Mic, pp. 1–14, 2009, doi: 10.1186/1471-2180-9-106.

[40] Y. Liu, T. Lehnert, and M. A. M. Gijs, "Fast antimicrobial susceptibility testing on: Escherichia coli by metabolic heat nanocalorimetry," *Lab on a Chip*, vol. 20, no. 17, pp. 3144–3157, 2020, doi: 10.1039/d0lc00579g.

[41] A. van Belkum *et al.*, "Developmental roadmap for antimicrobial susceptibility testing systems," *Nature Reviews Microbiology*, vol. 17, no. 1, pp. 51–62, 2019, doi: 10.1038/s41579-018-0098-9.

[42] M. Schrade, H. Fjeld, T. Norby, and T. G. Finstad, "Versatile apparatus for thermoelectric characterization of oxides at high temperatures," *Review of Scientific Instruments*, vol. 85, no. 10, 2014, doi: 10.1063/1.4897489.

[43] E. Kazura, B. R. Lubbers, E. Dawson, J. A. Phillips, and F. Baudenbacher, "Nano-Calorimetry based point of care biosensor for metabolic disease management," *Biomedical Microdevices*, vol. 19, no. 3, pp. 1–9, 2017, doi: 10.1007/s10544-017-0181-4.

[44] M. T. de Leon, H. Chong, and M. Kraft, “Solar thermoelectric generators fabricated on a silicon-on-insulator substrate,” *Journal of Micromechanics and Microengineering*, vol. 24, no. 8, 2014, doi: 10.1088/0960-1317/24/8/085011.

[45] T. Yamane, N. Nagai, S. I. Katayama, and M. Todoki, “Measurement of thermal conductivity of silicon dioxide thin films using a 3ω method,” *Journal of Applied Physics*, vol. 91, no. 12, pp. 9772–9776, 2002, doi: 10.1063/1.1481958.

[46] S. Franssila, L. Sainiemi, and M. Oy, “Encyclopedia of Microfluidics and Nanofluidics,” *Encyclopedia of Microfluidics and Nanofluidics*, pp. 1–13, 2013, doi: 10.1007/978-3-642-27758-0.

[47] K. C. Tang *et al.*, “Evaluation of bonding between oxygen plasma treated polydimethyl siloxane and passivated silicon,” *Journal of Physics: Conference Series*, vol. 34, no. 1, pp. 155–161, 2006, doi: 10.1088/1742-6596/34/1/026.

[48] R. Baillot and Y. Deshayes, “Tools and Analysis Methods of Encapsulated LEDs,” *Reliability Investigation of LED Devices for Public Light Applications*, pp. 43–106, 2017, doi: 10.1016/b978-1-78548-149-9.50002-x.